Int. J. Solids Structures Vol. 28, No. 9, pp. 1171–1184, 1991
Printed in Great Britain.

0020-7683/91 $3.00 + .00

BUCKLING AND POST-BUCKLING OF SYMMETRICALLY LAMINATED MODERATELY-THICK SPHERICAL CAPS

CHANG-SHI XU
Department of Civil Engineering, The University of Calgary, Calgary, Alberta, Canada T2N 1N4

(*Received* 27 *January* 1990; *in revised form* 10 *March* 1991)

Abstract—A non-linear shear-deformation theory is developed for the axisymmetric deformations of a shallow spherical cap comprising laminated cylindrically-orthotropic layers. Governing equations are expressed in terms of the transverse displacement, stress function and rotation. A Fourier–Bessel series solution is formulated for the post-buckling behaviour of symmetrically-laminated spherical thick caps with four types of edge conditions. Numerical results on the buckling and post-buckling behaviour of spherical caps under uniformly-distributed loads are presented for various boundary conditions, cap rises, base radius-to-thickness ratios, numbers of layers and material properties. The present results are compared with available data.

INTRODUCTION

The geometrically-non-linear behaviour of laminated composite structural members has received considerable attention in recent years. A number of researchers have studied the elastic behaviour of composite structures and have mainly focused on thin plates. A review of the literature on the geometric non-linear behaviour of composite plates may be found in references contributed by Chia (1980, 1988b) or elsewhere. Non-linear vibrations and post-buckling of laminated circular cylindrical shells were reported by Khot (1970a,b), Sheinman *et al.* (1983) and Iu and Chia (1988a,b) using various analytical methods. The non-linear axisymmetric response of orthotropic shallow spherical shells has been investigated in some detail. Using the Rayleigh–Ritz method, Varadan and Pandalai (1978) considered static buckling of orthotropic spherical caps based on a two-mode shape approximation. Alwar and Reddy (1979) and Dumir *et al.* (1984a) analyzed the static and dynamic buckling behavior of orthotropic shallow spherical caps with a circular hole using a Chebyshev series. Based on the collocation method, Dumir *et al.* (1984b) examined the static and dynamic buckling of orthotropic shallow spherical caps with an elastically-restrained edge. Utilizing a single-mode approximation, Dumir (1985) studied the non-linear axisymmetric response of orthotropic thin spherical caps on elastic foundations. Nath and Jain (1985a,b, 1986) employed a Chebyshev series to study the non-linear behaviour of orthotropic spherical caps, under conditions such as: the transient response, the influence of foundation mass on the non-linear damped response, static and dynamic response and the effect of an elastic foundation on the non-linear transient response. The non-linear static and dynamic responses of truncated conical and shallow spherical orthotropic shells were reported by Dumir (1986) making use of the Galerkin method. Recently, the non-linear vibrations and post-buckling of symmetrically-laminated shallow spherical shells with rectangular planform were discussed by Chia (1987, 1988a) utilizing a generalized double-Fourier series. All these analyses mentioned above, however, are confined to thin shells, and the effects of transverse shear deformation are neglected. In addition, a geometrically-non-linear analysis of laminated shallow sphericals caps by analytical methods cannot be found in the literature.

Several high-order theories of shells that take the effect of transverse shear deformation into account should be mentioned. Hildebrand *et al.* (1949) made a survey of various systems of equations for thin isotropic elastic shells and proposed a new system for orthotropic shells. On the basis of the work of Mindlin (1951) on the theory of isotropic plates, Herrmann and Mirsky (1956) derived a system of equations for isotropic circular cylindrical shells. Using Mindlin's theory and Love's approximation, Dong and Tso (1972) developed the

first shear-deformation theory for laminated orthotropic shells. Other contributions in this area were made by Whitney and Sun (1974) developing a linear refined theory for anisotropic shells, by Reddy and Liu (1985) formulating a linear higher-order shear deformation theory for laminated elastic shells, and by Stein (1986) proposing a non-linear shear-deformation theory for transverse isotropic shells.

In this paper, a non-linear shear-deformation theory is developed for axisymmetric deformation of laminated cross-ply shallow spherical caps. The buckling and post-buckling behaviour of symmetrically-laminated caps is studied. Governing equations are expressed in terms of a stress function, the rotation of a normal to the middle surface and the transverse displacement. These three dependent variables are expanded into Fourier–Bessel series, and governing equations are reduced to a set of algebraic equations by making use of the Galerkin method. Four types of edge conditions are considered. The results obtained for the buckling and post-buckling behaviour of symmetrically-laminated cross-ply spherical caps under a uniformly-distributed load are presented for various cap parameters and four types of boundary conditions.

BASIC EQUATIONS

Consider a shallow spherical cap (Fig. 1). The elevation of the middle surface of the cap above the base plane, f, is approximated by the paraboloid:

$$f = H[1-(r/a)^2] \tag{1}$$

where H is the initial rise of the spherical cap and a is the base radius. The radius of curvature of the undeformed cap is

$$R = a^2/(2H). \tag{2}$$

The cap, under the action of transverse forces of intensity $q(r)$, is assumed to consist of an arbitrary number of perfectly-bonded, cylindrically-orthotropic layers. Each layer has arbitrary thickness and elastic properties, and the axes of orthotropy of each layer coincide with the polar coordinates of the cap base plane. Within the framework of the shallow-shell theory ($H/a < 0.25$), the tangential forces and displacements can be taken to be their projections on the base plane of the shell, as proposed by Reissner (1946). With the transverse shear effect being taken into consideration, the radial displacement, u_r, at a distance z from the middle surface is assumed to vary linearly across the thickness of the cap and the transverse displacement is to remain constant. In the case of axisymmetric deformation of the shallow spherical cap, the displacement field may be written in the form (Iu and Chia, 1988b)

$$\begin{aligned} u_r(r,z) &= u(r)+z\psi(r) \\ u_\theta(r,z) &= 0 \\ w(r,z) &= w(r) \end{aligned} \tag{3}$$

in which u_r, u_θ and w are the displacements in the r, θ and z directions, respectively; u is the value of u_r at the middle surface and ψ is the rotation of a normal to the middle surface.

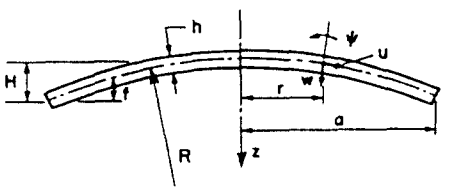

Fig. 1. Geometry and coordinate system of shallow spherical cap.

Neglecting the products of inplane-displacement derivatives, the classical non-linear strain–displacement relations become:

$$\varepsilon_r = \varepsilon_r^0 + z\kappa_r, \quad \varepsilon_\theta = \varepsilon_\theta^0 + z\kappa_\theta$$
$$\varepsilon_{rz} = \psi + w_{,r}, \quad \varepsilon_{\theta z} = \varepsilon_{r\theta} = \varepsilon_z = 0 \tag{4}$$

where a comma denotes differentiation with respect to the corresponding coordinate and where

$$\varepsilon_r^0 = u_{,r} - w/R + w_{,r}^2/2$$
$$\varepsilon_\theta^0 = u/r - w/R$$
$$\kappa_r = \psi_{,r}, \quad \kappa_\theta = \psi/r. \tag{5}$$

The stress–strain relations for the kth layer are

$$\begin{Bmatrix} \sigma_r^{(k)} \\ \sigma_\theta^{(k)} \end{Bmatrix} = \begin{bmatrix} S_{11}^{(k)} & S_{12}^{(k)} \\ S_{12}^{(k)} & S_{22}^{(k)} \end{bmatrix} \begin{Bmatrix} \varepsilon_r \\ \varepsilon_\theta \end{Bmatrix} \quad \sigma_{rz}^{(k)} = G_{rz}^{(k)} \varepsilon_{rz} \tag{6}$$

where $\sigma_r^{(k)}$, $\sigma_\theta^{(k)}$ and $\sigma_{rz}^{(k)}$ are the Kirchhoff stress components and $S_{ij}^{(k)}$ and $G_{rz}^{(k)}$ are the elastic in-plane and shear stiffness of the kth layer.

The stress and moment resultants are defined to be the same as in the classical shell theory. In view of (4) and (6), membrane stress and moment stress resultants are

$$\begin{Bmatrix} [N] \\ [M] \end{Bmatrix} = \begin{bmatrix} [A] & [B] \\ [B] & [D] \end{bmatrix} \begin{Bmatrix} [\varepsilon^0] \\ [\kappa] \end{Bmatrix} \tag{7}$$

where

$$[N] = \begin{Bmatrix} N_r \\ N_\theta \end{Bmatrix}, \quad [M] = \begin{Bmatrix} M_r \\ M_\theta \end{Bmatrix}, \quad [\varepsilon^0] = \begin{Bmatrix} \varepsilon_r^0 \\ \varepsilon_\theta^0 \end{Bmatrix}, \quad [\kappa] = \begin{Bmatrix} \kappa_r \\ \kappa_\theta \end{Bmatrix},$$
$$[A] = \begin{bmatrix} A_{11} & A_{12} \\ A_{12} & A_{22} \end{bmatrix}, \quad [B] = \begin{bmatrix} B_{11} & B_{12} \\ B_{12} & B_{22} \end{bmatrix}, \quad [D] = \begin{bmatrix} D_{11} & D_{12} \\ D_{12} & D_{22} \end{bmatrix}. \tag{8}$$

In these matrices, the elements A_{ij} and B_{ij} and D_{ij} are given by

$$(A_{ij}, B_{ij}, D_{ij}) = \int_{-h/2}^{h/2} S_{ij}^{(k)}(1, z, z^2)\, dz \quad (i, j = 1, 2). \tag{9}$$

The transverse shear strain in (4) represents the average shear strain across the thickness of the cap. As can be derived from the second of (6), the transverse shear stress is a step distribution across the cap thickness and does not vanish on the bounding surface of the cap. To eliminate this discrepancy a parabolic shear stress distribution across the cap thickness is assumed in the form as in the work by Fu and Chia (1989a,b):

$$\sigma_{rz} = \frac{3Q_r}{2h}\left[1 - \left(\frac{z}{h/2}\right)^2\right], \tag{10}$$†

and the transverse shear–stress resultant, Q_r, may be written as

† The displacement field assumed by Soldatos (1987) also yields a parabolic shear-stress distribution across the thickness of a laminate.

$$Q_r = G^*\varepsilon_{rz} = G^*(\psi + w_{,r}) \tag{11}$$

in which G^* is the shear rigidity. The complementary energy due to σ_{rz} given by expression (10) is

$$V = \frac{1}{2}\int_{-h/2}^{h/2} [(\sigma_{rz}^{(k)})^2/G_{rz}^{(k)}]\,\mathrm{d}z$$

$$= \frac{9Q_r^2}{8h^2}\sum_{k=1}^{N}\frac{1}{G_{rz}^{(k)}}\left[h_k - h_{k-1} - \frac{8}{3h^2}(h_k^3 - h_{k-1}^3) + \frac{16}{5h^4}(h_k^5 - h_{k-1}^5)\right] \tag{12}$$

where N is the number of layers. On the other hand, the complementary energy from expression (11) is

$$V = \tfrac{1}{2}Q_r^2/G^*. \tag{13}$$

Equating the shear complementary energies and hence coefficients of like terms yields

$$G^* = \frac{4h^2}{\sum_{k=1}^{N}\{9[(h_k - h_{k-1}) - 8(h_k^3 - h_{k-1}^3)/(3h^2) + 16(h_k^5 - h_{k-1}^5)/(5h^4)]/G_{rz}^{(k)}\}}. \tag{14}$$

Equation (7) gives the stress and moment resultants in terms of mid-surface strains and deformed cap curvatures. A partial inversion of this equation leads to

$$\begin{Bmatrix}[\varepsilon^0]\\ [M]\end{Bmatrix} = \begin{bmatrix}[A^*] & [B^*]\\ -[B^*]^{\mathrm{T}} & [D^*]\end{bmatrix}\begin{Bmatrix}[N]\\ [\kappa]\end{Bmatrix} \tag{15}$$

where the superscript T represents the matrix transpose and where

$$[A^*] = [A]^{-1}, \quad [B^*] = -[A]^{-1}[B], \quad [D^*] = [D] - [B][A]^{-1}[B]. \tag{16}$$

The equilibrium of in-plane stress and moment resultants and that of transverse forces require, in the absence of body forces,

$$\begin{aligned}(rN_r)_{,r} - N_\theta &= 0\\ rN_r(r/R + w_{,r}) + rQ_r + \int_0^r rq\,\mathrm{d}r &= 0\\ (rM_r)_{,r} - M_\theta - rQ_r &= 0\end{aligned} \tag{17}$$

in which q is the intensity of a distributed normal load.

By convection, a stress function, F, is introduced as

$$N_r = F/r, \quad N_\theta = F_{,r}. \tag{18}$$

This function satisfies the first of (17) exactly. Using (11) and (15), the last two of (17) and the compatibility condition, the resulting equations may be written in the following dimensionless form:

$$-\lambda_1\bar{B}_{21}\rho\bar{F}_{,\rho\rho} - \lambda_1(\bar{B}_{11} + \bar{B}_{21} - \bar{B}_{22})\bar{F}_{,\rho} + \lambda_1\bar{B}_{12}\bar{F}/\rho + \bar{D}_{11}(\bar{\psi}_{,\rho} + \rho\bar{\psi}_{,\rho\rho})$$

$$-\bar{D}_{22}\bar{\psi}/\rho + 2\lambda_1^2\lambda_2\rho\bar{F} + \lambda_1\bar{F}W_{,\rho} + \lambda_1^2\lambda_2^2\int_0^\rho \rho Q\,\mathrm{d}\rho = 0$$

$$T_s[-\lambda_1\bar{B}_{21}\rho\bar{F}_{,\rho\rho}-\lambda_1(\bar{B}_{11}+\bar{B}_{21}-\bar{B}_{22})\bar{F}_{,\rho}+\lambda_1\bar{B}_{12}\bar{F}/\rho+\bar{D}_{11}(\bar{\psi}_{,\rho}+\rho\psi_{,\rho\rho})$$
$$-\bar{D}_{22}\bar{\psi}/\rho]-\lambda_1^2\bar{G}\rho(\bar{\psi}+W_{,\rho})=0$$
$$\bar{A}_{22}(\rho\bar{F}_{,\rho\rho}+\bar{F}_{,\rho})-\bar{A}_{11}\bar{F}/\rho+\bar{B}_{21}\rho\bar{\psi}_{,\rho\rho}/\lambda_1+(\bar{B}_{21}+\bar{B}_{22}-\bar{B}_{11})\bar{\psi}_{,\rho}/\lambda_1$$
$$-\bar{B}_{12}\bar{\psi}/(\lambda_1\rho)+2\lambda_2\rho W_{,\rho}+W_{,\rho}^2/(2\lambda_1)=0. \quad (19)$$

In the above equations, T_s is a tracing constant, which represents the influence of transverse shear when $T_s=1$; when $T_s=0$, this effect is neglected. Also in these equations, the dimensionless parameters are defined as:

$$\rho=r/a,\quad W=w/h,\quad \bar{\psi}=(a/h)\psi,\quad \bar{F}=F/(E_rh^2)$$
$$\lambda_1=a/h,\quad \lambda_2=H/a,\quad Q=qa^4/(E_rh^2H^2)$$
$$\bar{A}_{ij}=A_{ij}^*E_rh,\quad \bar{B}_{ij}=B_{ij}^*/h,\quad \bar{D}_{ij}=D_{ij}^*/(E_rh^3)\quad (i,j=1,2)$$
$$\bar{G}=G^*/(E_rh). \quad (20)$$

Including the transverse shear deformation, the resulting eqns (19) constitute a system of equations governing the axisymmetric finite deformation of an unsymmetrically-laminated spherical cap comprising cylindrically-orthotropic layers.

In what follows, the present study is restricted to a cross-ply spherical cap laminated symmetrically with respect to the middle surface, for which

$$B_{ij}^*=0,\quad D_{ij}^*=D_{ij}\quad (i,j=1,2). \quad (21)$$

The resulting eqns (19) thus are simplified to

$$\bar{D}_{11}(\bar{\psi}+\rho\bar{\psi}_{,\rho\rho})-\bar{D}_{22}\bar{\psi}/\rho+2\lambda_1^2\lambda_2\rho\bar{F}+\lambda_1\bar{F}W_{,\rho}+\lambda_1^2\lambda_2^2\int_0^\rho\rho Q\,\mathrm{d}\rho=0$$
$$T_s[\bar{D}_{11}(\bar{\psi}_{,\rho}+\rho\bar{\psi}_{,\rho\rho})-\bar{D}_{22}\bar{\psi}/\rho]-\lambda_1^2\bar{G}\rho(\bar{\psi}+W_{,\rho})=0$$
$$\bar{A}_{22}(\rho\bar{F}_{,\rho\rho}+\bar{F}_{,\rho})-\bar{A}_{11}\bar{F}/\rho+2\lambda_2\rho W_{,\rho}+W_{,\rho}^2/(2\lambda_1)=0. \quad (22)$$

To formulate a solution to the present problem, two finite conditions at the apex should be imposed to ensure that stress couples and membrane stress resultants do not increase indefinitely at the apex:

$$\bar{\psi}=0\quad\text{and}\quad N_\rho(=\bar{F}/\rho)\quad\text{is finite at}\ \rho=0. \quad (23)$$

Four types of boundary conditions at the edge are also considered and expressed in dimensionless form:

(i) For a clamped immovable edge (CI):

$$W=0,\quad \bar{\psi}=0,\quad U=\bar{A}_{12}\bar{F}+\bar{A}_{22}\rho\bar{F}_{,\rho}=0\quad\text{at}\quad\rho=1. \quad (24)$$

(ii) For a clamped movable edge (CM):

$$W=0,\quad \bar{\psi}=0,\quad N_\rho=0\quad\text{at}\quad\rho=1. \quad (25)$$

(iii) For a simply-supported movable edge (SM):

$$W=0,\quad M_\rho=\bar{D}_{11}\bar{\psi}_{,\rho}+\bar{D}_{12}\bar{\psi}/\rho=0,\quad N_\rho=0\quad\text{at}\quad\rho=1. \quad (26)$$

(iv) For a simply-supported immovable edge (SI):

$$W = 0, \quad M_\rho = 0, \quad U = 0 \quad \text{at} \quad \rho = 1 \tag{27}$$

where

$$M_\rho = M_r a^2/(E_r h^4), \quad N_\rho = N_r a/(E_r h^2), \quad U = u/h. \tag{28}$$

The system of (22) is to be solved in conjunction with finite conditions (23) and boundary conditions (24)–(27), respectively.

METHOD OF SOLUTION

A solution to the system of (22) is formulated by expansion of dependent variables W, $\bar{\psi}$ and $\bar{F}$ into Fourier–Bessel series:

$$\begin{aligned} W &= \sum_{m=1}^{\infty} W_m X_m(\rho) \\ \bar{\psi} &= \sum_{m=1}^{\infty} R_m Y_m(\rho) \\ \bar{F} &= \sum_{r=1}^{\infty} S_r Z_r(\rho). \end{aligned} \tag{29}$$

In these expressions, W_m, R_m and S_r are constant coefficients to be determined later and functions X_m, Y_m and Z_r are given by:

$$\begin{aligned} X_m(\rho) &= J_0(\alpha_m\rho) - I_0(\alpha_m\rho)J_0(\alpha_m)/I_0(\alpha_m) \\ Y_m(\rho) &= J_1(\alpha_m\rho) + I_1(\alpha_m\rho)J_0(\alpha_m)/I_0(\alpha_m) \\ Z_r(\rho) &= \rho J_0(\beta_r\rho) \end{aligned} \tag{30}$$

where J_0, J_1, I_0 and I_1 are Bessel functions and modified Bessel functions of the first kind of order zero and order one. The condition $W = 0$ at the edge and the finite conditions at the apex are automatically satisfied by the assumed solution (29). The constants α_m and β_r are determined by substituting the expressions for $\bar{\psi}$ and $\bar{F}$ into the last two in each set of boundary conditions (24)–(27). The values of these constants are presented in Table 1, with elastic constants typical of glass–epoxy, boron–epoxy and graphite–epoxy composite

Table 1. Values of α_k and β_k in eqns (30)

	Boundary condition	Material	N	$k = 1$	$k = 2$	$k = 3$
	Clamped			3.1962206	6.3064370	9.4394991
α_k	Simply supported	ISO	1	2.2488001	5.4604944	8.6167405
		GL	3	2.2731447	5.4687601	8.6217531
		BO	3	2.2045701	5.4462973	8.6082163
		GR	3	2.1652488	5.4345622	8.6012501
β_k	Immovable	ISO	1	1.0292778	3.9877522	7.1024909
		GL	3	1.0872543	4.0084519	7.1143470
		BO	3	1.2136517	4.0600777	7.1443501
		GR	3	1.2376280	4.0709737	7.1507681
	Movable			2.4048256	5.5200781	8.6537279

Table 2. Numerical values of elastic constants

Material	E_θ/E_r	G_{rz}/E	$\nu_{\theta r}$
Glass–epoxy (GL)	3	0.5	0.25
Boron–epoxy (BO)	10	0.333	0.22
Graphite–epoxy (GR)	16	0.22	0.30
Isotropic (ISO)	1	0.385	0.30

materials. These elastic constants are given in Table 2, where E_r and E_θ are the principal moduli of elasticity of an orthotropic material, G_{rz} is the shear modulus, and $\nu_{\theta r}$ is the Poisson ratio.

Substituting series (29) into (22), multiplying the first of (22) by $X_n(\rho)$, the second by $Y_n(\rho)$ and the third by $Z_s(\rho)$, and then integrating with respect to ρ from 0 to 1, we obtain the following three sets of algebraic equations for W_m, R_m and S_r:

$$\begin{aligned} a^{mr}_{1n} W_m S_r + a^m_{2n} R_m + a^r_{3n} S_r + a_{4n} Q &= 0 \\ a^m_{5n} R_m + a^m_{6n} W_m &= 0 \\ a^r_{7s} S_r + a^m_{8s} W_m + a^{mk}_{9s} W_m W_k &= 0 \end{aligned} \tag{31}$$

in which Q is the load parameter for q (being a uniform external normal pressure), and the as are constants presented in the Appendix. For simplification in calculation, coefficients R_m and S_r can be expressed in terms of W_m from the last two of (31):

$$\begin{aligned} R_m &= -[a^m_{5q}]^{-1} a^k_{6q} W_k \\ S_r &= -[a^r_{7s}]^{-1} a^k_{8s} W_k - [a^r_{7s}]^{-1} a^{mk}_{9s} W_m W_k. \end{aligned} \tag{32}$$

Substituting (32) into the first of (31), the resulting equation for W_m is

$$b^m_{1n} W_m + b^{mk}_{2n} W_m W_k + b^{mkj}_{3n} W_m W_k W_j + a_{4n} Q = 0 \tag{33}$$

where the bs are constants also given in the Appendix. This system of simultaneous non-linear algebraic equations for the Fourier–Bessel coefficients W_m can be handled systematically by a computer for an arbitrary number of terms in these truncated series (29).

NUMERICAL RESULTS AND DISCUSSIONS

Computations were performed for a symmetrically-laminated cross-ply spherical thick cap which consists of an odd number of cylindrically-orthotropic layers, all of the same thickness and material properties. Elastic constants used in calculation are presented in Table 2 for glass–epoxy (GL), boron–epoxy (BO) and graphite–epoxy (GR) composite materials and for an isotropic material. Uniformly-distributed static loading normal to the undeformed middle surface is assumed. In calculation, only the first three terms in each truncated series for W, $\bar{\psi}$ and $\bar{F}$ in (29) are taken into account because numerical results have demonstrated that the influence of the other terms is negligibly small. The results are presented in graphs and tables for the dimensionless load, Q, and maximum deflection, w_{max}/h. In addition the average dimensionless deflection, $\bar{W}$ is introduced in order to compare with the previous results obtained by Dumir *et al* (1984b):

$$\bar{W} = 2\int_0^1 \rho W \, d\rho. \tag{34}$$

The numerical procedure is briefly described for solving the set of non-linear algebraic eqns (33) for Q and W_m in the truncated series (29) by the Newton–Raphson method. The number of non-linear algebraic equations is equal to the number of unknowns for any

Table 3. Comparison of values of $(H/a)_{cr}$ and Q_{cr}

	Present ($T_s = 0$)		Varadan and Pandalai (1978)	
$\nu_{\theta r} = 1/3$	$(H/a)_{cr}$	Q_{cr}	$(H/a)_{cr}$	Q_{cr}
$E_\theta/E_r = 1$ (CI)	0.08305	3.1802	0.08248	3.2152
$E_\theta/E_r = 4$ (CI)	0.09720	4.7172	0.10010	4.8170

truncated series. By prescribing one of the unknowns W_m or Q, the resulting non-linear algebraic equations can be readily solved provided that a good initial guess be made for the other unknown. In general, the prescribed value is one of W_m while the initial guess is the previous solution. The difference between the prescribed unknown and the corresponding unknown in the previous solution should be made small to ensure rapid convergence. The maximum number of iterations required for convergence is 10. Once a solution for the Fourier–Bessel coefficents W_m and load Q is obtained, the maximum deflection w_{max} at the pole can easily be determined.

In this study the least value of the geometric parameter, H/a, denoted by $(H/a)_{cr}$, for which buckling occurs is obtained by use of the foregoing procedure. The value of the ratio H/a for which buckling does not occur is increased by a small increment and (33) is solved. The process is repeated until buckling just occurs and vice versa until buckling just disappears. The values of $(H/a)_{cr}$ and the associated buckling loads for isotropic and orthotropic immovable clamped spherical caps are presented in Table 3 for comparison with those given by Varadan and Pandalai (1978). The maximum difference between two sets of values is less than 3%.

As a partial check on the accuracy of the present solution, the load–deflection curves of isotropic and orthotropic thin spherical caps with simply-supported immovable and movable edges (SI and SM) for various values of the modulus ratio are compared in Fig. 2 with those obtained by Dumir (1985) using the orthogonal point collocation method. A good agreement is observed between the two sets of curves. In Fig. 3, the present results for the post-buckling behaviour of clamped immovable orthotropic spherical caps with different cap rises agree closely with those given by Dumir *et al.* (1984b). A comparison of buckling loads is shown in Fig. 4 for isotropic spherical caps with immovable clamped and simply-supported edges. Present results obtained by neglecting the transverse shear are represented by solid curves ($T_s = 0$) and those taking this effect into account by dotted curves ($T_s = 1$). The present results obtained by neglecting the transverse shear effect are in good agreement with those given by Varadan and Pandalai (1978) for a clamped edge and by Dumir *et al.* (1984) for a simply-supported edge. The effects of material properties on the values of $(H/a)_{cr}$ and Q_{cr} shown in Fig. 5 are presented in Table 4. The value of

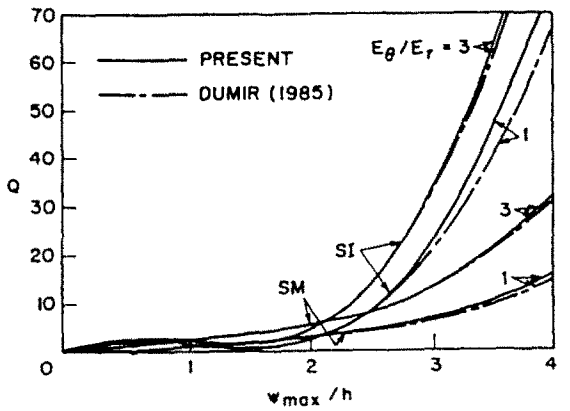

Fig. 2. Comparison of load–deflection response for simply-supported isotropic and orthotropic spherical caps ($\nu_{\theta r} = 0.3$, $a/h = 50$, $H/a = 0.02$).

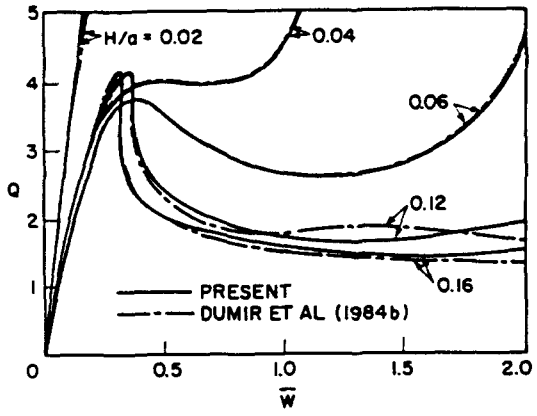

Fig. 3. Comparison of buckling and post-buckling behaviour for clamped immovable (CI) orthotropic spherical cap with different cap rises ($E_\theta/E_r = 3$, $\nu_{\theta r} = 0.3$, $a/h = 50$).

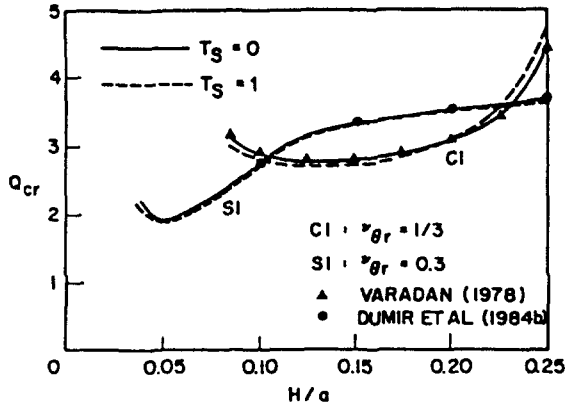

Fig. 4. Comparison of buckling loads for clamped immovable (CI) and simply-supported immovable (SI) isotropic spherical cap for $a/h = 20$.

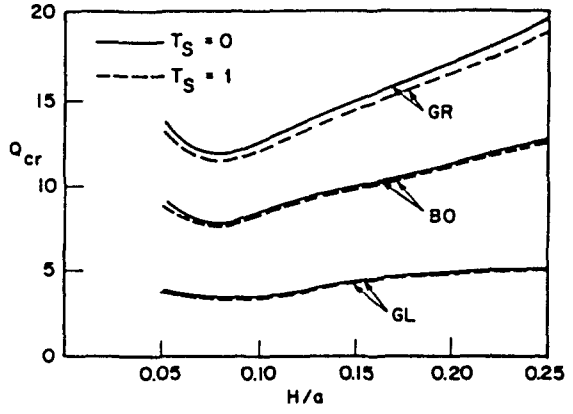

Fig. 5. Effect of material properties on buckling loads of simply-supported immovable three-layer spherical cap for $a/h = 15$.

$(H/a)_{cr}$ is roughly 0.05 for a simply-supported immovable three-layer cross-ply spherical cap with $a/h = 15$. By inspecting these curves, it may be noted that the buckling load Q_{cr} initially decreases and then increases with an increase in the ratio H/a. Figure 5 also indicates that for a symmetrically-laminated cross-ply spherical cap, the buckling load Q_{cr} increases with an increasing modulus ratio, but the critical value $(H/a)_{cr}$ decreases as the ratio increases.

Table 4. Values of $(H/a)_{cr}$ and Q_{cr} shown in Fig. 5

Material	$T_s = 0$		$T_s = 1$	
	$(H/a)_{cr}$	Q_{cr}	$(H/a)_{cr}$	Q_{cr}
GL	0.05414	3.9635	0.05393	3.9478
BO	0.05246	9.1398	0.05168	9.0142
GR	0.05197	13.6390	0.05037	13.2362

Figure 6 shows the post-buckling response of a clamped cross-ply spherical cap for various values of H/a. It can be seen from these response curves that, except for when $H/a = 0.1$, all caps undergo snap-through buckling and have a reduction in load after buckling. The buckling load increases as the ratio H/a increases. The maximum deflection of a clamped immovable cross-ply cap is plotted in Fig. 7 against the transverse load for different materials. With the transverse shear effect neglected, the snap-through buckling of all caps of different materials occurs at approximately the maximum deflection equal to the cap thickness.

The response curves for simply-supported movable three-layer cross-ply caps are shown in Fig. 8 for different ratios of the base radius-to-thickness. It is found that the buckling load increases with this ratio. In Fig. 9 the effect of the number of layers N on the buckling load is illustrated for clamped movable cross-ply caps. These curves indicate that the buckling load increases as the number of layers increases. For the value $N \leqslant 5$ the influence of the number of layers on the buckling load is much pronounced. The buckling load increases by 60% when N is changed from $N = 1$ (orthotropic cap) to $N = 15$. This increase

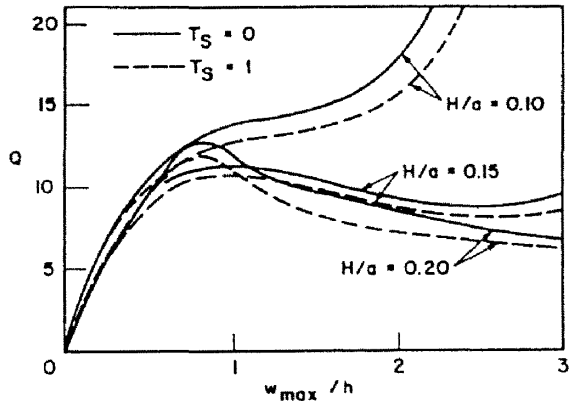

Fig. 6. Effect of cap height on post-buckling response of clamped immovable five-layer boron epoxy spherical cap for $a/h = 15$.

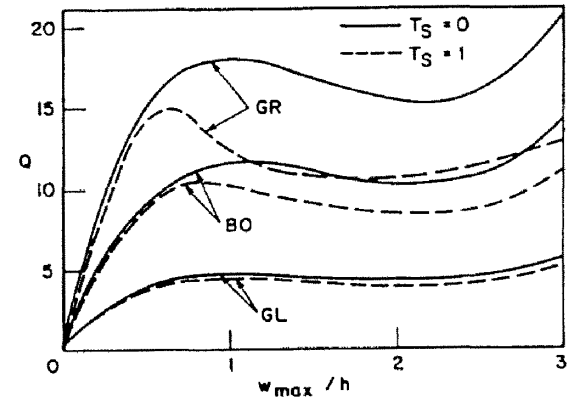

Fig. 7. Effect of material properties on post-buckling response of clamped immovable five-layer spherical cap for $a/h = 10$ and $H/a = 0.2$.

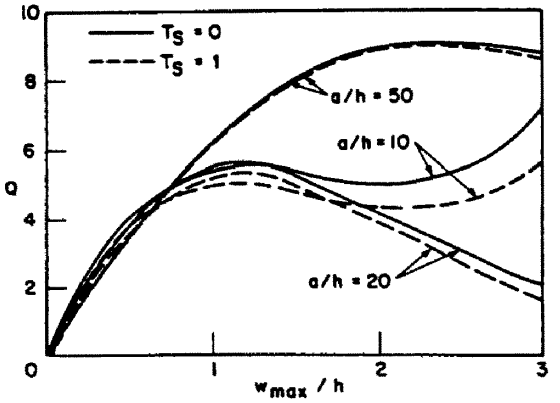

Fig. 8. Effect of base radius-to-thickness ratio on post-buckling response of simply-supported movable three-layer graphite–epoxy spherical cap for $H/a = 0.2$.

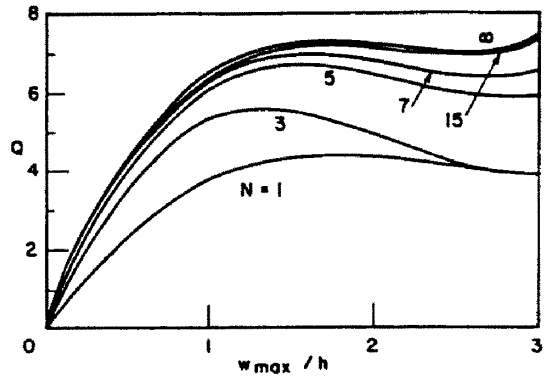

Fig. 9. Effect of number of layers on post-buckling response of clamped movable boron–epoxy spherical cap ($a/h = 50$, $H/a = 0.06$ and $T_s = 0$).

is considerably significant for the load-carrying capacity. The load–deflection curves shown in Fig. 10 depict the effect of edge conditions on the buckling load of a five-layer cap. It is observed that the effect of in-plane edge conditions is much noticeable. For the clamped cap the buckling load is 80% greater with an immovable edge than with a movable edge; for a simply-supported cap, it is 240% greater. The buckling loads of clamped and simply-supported caps are nearly the same for edges immovable in the meridian direction, but are different by 90% for movable edges.

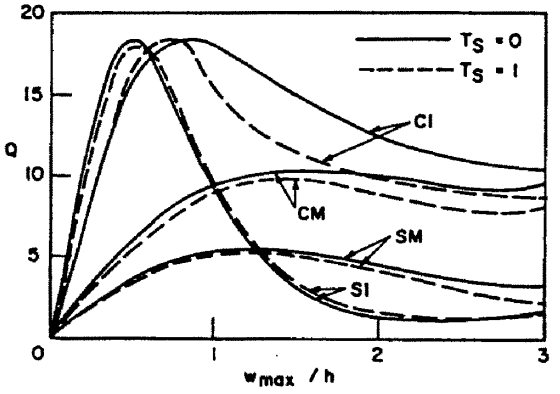

Fig. 10. Effect of edge condition on the post-buckling response of five-layer graphite–epoxy spherical cap for $a/h = 15$ and $H/a = 0.2$.

In this analysis, the effect of transverse shear on the buckling and post-buckling behaviour of laminated spherical caps is also studied in some detail. In Figs 4-8 and 10 all dotted curves take into account this effect, for comparison with solid curves neglecting this effect. These results indicate that the effect of transverse shear does not alter the behaviour of the elastic response, but in all cases generally results in a reduction in the buckling load and post-buckling load-carrying capacity. This reduction is more pronounced for high-modulus composite materials as shown in Figs 5 and 7. For clamped immovable five-layer caps comprised of glass–epoxy, boron–epoxy and graphite–epoxy materials, the effect of transverse shear reduces the buckling load by 4%, 11% and 18%, respectively, as depicted in Fig. 7. The reduction in the post-buckling load caused by the effect is 35% at $w_{max}/h = 1.2$ in the case of the graphite–epoxy material. As shown in Fig. 8, the transverse shear deformation exhibits a strong influence on the buckling and post-buckling behaviour for moderately-thick laminated spherical caps and the buckling load is reduced by 10.3% for $a/h = 10$. It is noticed that a large reduction in buckling and post-buckling loads shown in Fig. 7 is partially due to the small ratio of the base radius-to-thickness, i.e. $a/h = 10$. The reduction, however, is not significant for large values of this ratio such as $a/h = 50$, as shown in Fig. 8. The effect of the transverse shear on buckling load and post-buckling response of a five-layer graphite–epoxy spherical cap is illustrated in Fig. 10 for four types of boundary conditions. The reduction in the post-buckling load caused by this effect is much more significant for a clamped immovable cap than for clamped and simply-supported movable caps. In the case of a simply-supported movable cap, the transverse shear effect slightly increases the post-buckling load rather than decreases it.

CONCLUSION

Governing equations including the transverse shear deformation are derived for the axisymmetric finite deformation of a spherical cap comprising laminated cylindrically-orthotropic layers. A solution is formulated for the buckling and post-buckling of a symmetrically-laminated cross-ply spherical cap under uniform normal pressure for four types of edge conditions. In special cases, present results are in good agreement with those suggested by other studies. Numerical results are presented graphically for various values of cap rise, base radius-to-thickness ratio, number of layers and material properties and for different boundary conditions. Based on this study some concluding remarks may be drawn.

The buckling load of a laminated spherical cap increases with the increase in the modulus ratio, the base radius-to-thickness ratio and the number of layers, but decreases with the increase in the ratio of the cap rise to base radius. Once the least value of this ratio H/a occurs, the buckling load initially decreases and then increases with an increase in the ratio. For the four types of edge conditions considered, the effect of in-plane conditions on the buckling load is much noticeable, especially for the simply-supported edge. The load-carrying capacity in the post-buckling range increases with the increase in the number of layers and in the modulus ratio of a composite material.

The transverse shear effect is significant especially for a moderately-thick and laminated spherical cap and generally reduces the buckling and post-buckling loads. The effect, however, does not change the general behaviour of the cap response in all cases. The effect of transverse shear on the buckling is pronounced for caps of high-modulus materials and caps with low base radius-to-thickness ratios. For a moderately-thick spherical laminate the effect on post-buckling behaviour is considerably remarkable. This effect on the load-carrying capacity is greater for caps with a clamped edge than for that with simply-supported edge.

Acknowledgement—The results presented in this paper were obtained in the course of research sponsored by the Natural Science and Engineering Research Council of Canada.

REFERENCES

Alwar, R. S. and Reddy, B. S. (1979). Dynamic buckling of isotropic and orthotropic shallow spherical cap with circular hole. *Int. J. Mech. Sci.* **21**, 681–688.

Chia, C. Y. (1980). *Nonlinear Analysis of Plates*. McGraw-Hill, New York.
Chia, C. Y. (1987). Large amplitude vibration of geometrically imperfect symmetrically laminated shallow spherical shell with elastically restrained edges. *Proc. 6th Int. Conf. on Composites Materials and 2nd European Conf. on Composites Materials*. Vol. 5, pp. 90–100. Elsevier Applied Science, Amsterdam.
Chia, C. Y. (1988a). Nonlinear analysis of doubly curved symmetrically laminated shallow shells with rectangular planform. *Ing.-Arch.* **58**, 252–264.
Chia, C. Y. (1988b). Geometrically nonlinear behaviour of composite plates: a review. *Appl. Mech. Rev.* **41**, 439–451.
Dong, S. B. and Tso, F. K. W. (1972). On a laminated orthotropic shell theory including transverse shear deformation. *J. Appl. Mech.* **39**, 1091–1097.
Dumir, P. C. (1985). Nonlinear axisymmetric response of orthotropic thin spherical caps on elastic foundation. *Int. J. Mech. Sci.* **27**, 751–760.
Dumir, P. C. (1986). Nonlinear axisymmetric response of orthotropic thin truncated conical and spherical caps. *Acta Mech.* **60**, 121–132.
Dumir, P. C., Gandhi, M. L. and Nath, Y. (1984a). Axisymmetrical static and dynamic buckling of orthotropic shallow spherical caps with circular hole. *Comput. Struct.* **19**, 725–736.
Dumir, P. C., Gandhi, M. L. and Nath, Y. (1984b). Axisymmetric static and dynamic buckling of orthotropic shallow spherical caps with flexible support. *Acta Mech.* **52**, 93–106.
Fu, Y. M. and Chia, C. Y. (1989a). Multi-mode non-linear vibration and postbuckling of anti-symmetric imperfect angle-ply cylindrical thick panels. *Int. J. Nonlinear Mech.* **24**, 365–381.
Fu, Y. M. and Chia, C. Y. (1989b). Nonlinear analysis of unsymmetrically laminated imperfect thick panels on elastic foundation. *Compos. Struct.* **13**, 289–314.
Herrmann, G. and Mirsky, I. (1956). Three-dimensional and shell-theory analysis of axially symmetric motions of cylinders. *J. Appl. Mech.* **23**, 563–568.
Hildebrand, F. B., Reissner, E. and Thomas, G. B. (1949). Notes on the foundations of the theory of small displacements of orthotropic shells. NACA TN 1833.
Iu, V. P. and Chia, C. Y. (1988a). Non-linear vibration and postbuckling of unsymmetric cross-ply circular cylindrical shells. *Int. J. Solids Structures* **24**, 195–210.
Iu, V. P. and Chia, C. Y. (1988b). Effect of transverse shear on nonlinear vibration and postbuckling of anti-symmetric cross-ply imperfect cylindrical shells. *Int. J. Mech. Sci.* **30**, 705–718.
Khot, N. S. (1970a). Buckling and postbuckling behavior of composite cylindrical shells under axial compression. *AIAA Jl* **8**, 229–235.
Khot, N. S. (1970b). Postbuckling behavior of geometrically imperfect composite cylindrical shells under axial compression. *AIAA Jl* **8**, 579–581.
Mindlin, R. D. (1951). Influence of rotatory inertia and shear on flexural motions of isotropic, elastic plates. *J. Appl. Mech.* **18**, 31–38.
Nath, Y. and Jain, R. K. (1985a). Influence of foundation mass on the nonlinear damped response of orthotropic shallow spherical shells. *Int. J. Mech. Sci.* **27**, 471–479.
Nath, Y. and Jain, R. K. (1985b). Orthotropic annular shells on elastic foundations. *ASCE J. Engng Mech.* **111**, 1242–1256.
Nath, Y. and Jain, R. K. (1986). Nonlinear studies of orthotropic shallow spherical shells on elastic foundation. *Int. J. Nonlinear Mech.* **21**, 447–458.
Reddy, J. N. and Liu, C. F. (1985). A higher-order shear deformation theory of laminated elastic shells. *Int. J. Engng Sci.* **23**, 319–330.
Reissner, E. (1946). Stresses and small displacements of shallow spherical shells: I. *J. Math. Phys.* **25**, 80–85.
Sheinman, I., Shaw, D. and Simitses, G. J. (1983). Nonlinear analysis of axially-loaded laminated cylindrical shells. *Comput. Struct.* **16**, 131–137.
Soldatos, K. P. (1987). Influence of thickness shear deformation on free vibrations of rectangular plates, cylindrical panels and cylinders of antisymmetric angle-ply construction. *J. Sound. Vib.* **119**, 111–137.
Stein, M. (1986). Nonlinear theory for plates and shells including the effects of transverse shearing. *AIAA Jl* **24**, 1537–1544.
Varadan, T. K. and Pandalai, K. A. V. (1978). Nonlinear flexural oscillations of orthotropic shallow spherical shells. *Comput. Struct.* **9**, 417–425.
Whitney, J. M. and Sun, C. T. (1974). A refined theory for laminated anisotropic, cylindrical shells. *J. Appl. Mech.* **41**, 471–476.

APPENDIX

$$a_{1n}^{rr} = \lambda_1 \int_0^1 X_n X_m' Z_r \, d\rho$$

$$a_{2n}^{m} = \int_0^1 (\bar{D}_{11} X_n Y_m' + \bar{D}_{11} \rho X_n Y_m'' - \bar{D}_{22} X_n Y_m/\rho) \, d\rho$$

$$a_{3n}^{r} = 2\lambda_1^2 \lambda_2 \int_0^1 \rho X_n Z_r \, d\rho$$

$$a_{4n} = \tfrac{1}{2}\lambda_1^2 \lambda_2^2 \int_0^1 \rho^2 X_n \, d\rho$$

$$a^m_{5n} = T_r \int_0^1 (\bar{D}_{11} Y_n Y'_m + \bar{D}_{11} \rho Y_n Y''_m - \bar{D}_{22} Y_n Y_m / \rho)\, \mathrm{d}\rho - \lambda_1^2 \bar{G} \int_0^1 \rho Y_n Y_m \, \mathrm{d}\rho$$

$$a^m_{6n} = -\lambda_1^2 \bar{G} \int_0^1 \rho Y_n X'_m \, \mathrm{d}\rho$$

$$a'_{7r} = \int_0^1 (\bar{A}_{22} \rho Z_r Z''_r + \bar{A}_{22} Z_r Z'_r - \bar{A}_{11} Z_r Z_r / \rho)\, \mathrm{d}\rho$$

$$a^m_{8r} = 2\lambda_2 \int_0^1 \rho Z_r X'_m \, \mathrm{d}\rho$$

$$a^{mk}_{9r} = \frac{1}{2\lambda_1} \int_0^1 Z_r X_m X_k \, \mathrm{d}\rho$$

$$b^m_{1n} = -a^2_{2n} [a^2_{5q}]^{-1} a^m_{6q} - a'_{3n} [a'_{7r}]^{-1} a^m_{8r}$$

$$b^{mk}_{2n} = -a^{kr}_{1n} [a'_{7r}]^{-1} a^m_{8r} - a'_{3n} [a'_{7r}]^{-1} a^{mk}_{9r}$$

$$b^{mkl}_{3n} = a^{lr}_{1n} [a'_{7r}]^{-1} a^{mk}_{9r}$$

in which primes denote differentiation with respect to the corresponding coordinate.